Wind and Structures, *Vol. 24, No. 2 (2017) 145-169*
DOI: https://doi.org/10.12989/was.2017.24.2.145

Effects of vertical ribs protruding from facades on the wind loads of super high-rise buildings

Yong Quan[a], Fangchao Hou[b] and Ming Gu[*]

State Key Laboratory of Disaster Reduction in Civil Engineering, Tongji University, Shanghai 200092, China

(Received July 16, 2016, Revised November 28, 2016, Accepted December 2, 2016)

Abstract. The auxiliary structures of a high-rise building, such as balconies, ribs, and grids, are usually much smaller than the whole building; therefore, it is difficult to simulate them on a scaled model during wind tunnel tests, and they are often ignored. However, they may have notable effects on the local or overall wind loads of the building. In the present study, a series of wind pressure wind tunnel tests and high-frequency force balance (HFFB) wind tunnel tests were conducted on rigid models of an actual super high-rise building with vertical ribs protruding from its facades. The effects of the depth and spacing of vertical ribs on the mean values, fluctuating values and the most unfavorable values of the local wind pressure coefficients were investigated by analyzing the distribution of wind pressure coefficients on the facades and the variations of the wind pressure coefficients at the cross section at 2/3 of the building height versus wind direction angle. In addition, the effects of the depth and spacing of vertical ribs on the mean values, fluctuating values and power spectra of the overall aerodynamic force coefficients were studied by analyzing the aerodynamic base moment coefficients. The results show that vertical ribs significantly decrease the most unfavorable suction coefficients in the corner recession regions and edge regions of facades and increase the mean and fluctuating along-wind overall aerodynamic forces.

Keywords: vertical ribs; wind pressure; aerodynamic force; high-rise building; wind tunnel test

1. Introduction

The aerodynamic shapes of high-rise buildings significantly affect the wind load. Kwok (1988), Kwok, Wilhelm *et al*. (1988) investigated the effects of horizontal slots, slotted corners and chamfered corners on the wind-induced response of a tall building with a rectangular cross section. Kawai (1998) analyzed the effects of corner cut, recession and roundness on aeroelastic instabilities. Gu and Quan (2004), Quan, Gu *et al*. (2005), Gu, Cao *et al*. (2014) studied the effects of corner recessions, chamfered corners and tapered sections on the across-wind aerodynamic damping through a series of wind tunnel tests. Kim and Kanda (2010a, b) researched the effects of section taper and setback on the wind-induced response of high-rise buildings. These findings suggest that some seemingly minor changes in the corners and facades of a building may significantly change the local wind pressures and the overall aerodynamic forces.

∗Corresponding author, Professor, E-mail: minggu@tongji.edu.cn
[a] Professor, Email: quanyong@tongji.edu.cn
[b] Ph.D. Student, Email: fangchaohou@163.com

http://www.techno-press.org/?journal=was&subpage=8 ISSN: 1226-6116 (Print), 1598-6225 (Online)

All of the above studies were based on high-rise building models with smooth surfaces. However, to improve appearance or for practical functions, some buildings are designed with grids, balconies, ribs or other auxiliary structures on their facades. These auxiliary structures not only make the facades rough but also change the overall aerodynamic shape of the building. Compared with the whole building, these auxiliaries are usually too small to be simulated in wind tunnel test models, so few researchers have systematically studied the impact of these small changes on the wind loads of a high-rise building. Naudascher, Weske *et al.* (1981) studied the effects of different rib spacing on the across-wind aerodynamic damping of tall, square buildings. The results indicated that appropriate ribs can effectively weaken the across-wind vortex-induced vibration and change the galloping damping, which can partially or completely suppress galloping vibration. Quan, Kuang *et al.* (2015) investigated the effects of grid curtains on the wind loads of the main structure and facades of a high-rise building using rigid model wind pressure wind tunnel tests and high-frequency force balance wind tunnel tests. This research found that grid curtains slightly affect the mean and fluctuating wind pressures on the windward facade but greatly reduce the high negative wind pressure on the sideward facade. Grid curtains increase the mean and fluctuating aerodynamic along-wind forces and decrease the fluctuating aerodynamic torsions, mainly affecting the wind forces in the low-frequency range.

In the present study, the effects of the depth and spacing of vertical ribs protruding from facades on the local wind pressure and total aerodynamic forces of an actual super high-rise building are investigated based on a series of wind pressure wind tunnel tests and high-frequency force balance wind tunnel tests on rigid models.

2. Outline of the building and the wind tunnel tests

2.1 General building information

This study was based on wind tunnel tests using rigid models of an actual super high-rise building with a height of 224.7 m, as shown in Fig. 1. The cross section of this building is a slightly curved square with corner recessions. The cross section at 2/3 of the total building height is shown in Fig. 2. The width of the building, W, is approximately 52.3 m, and changes only slightly along the height. The size of the corner recession is 5.01 m, approximately $9.6\%W$, and the width of the curtain facades, B, is approximately 42.28 m. The depth of the vertical ribs is 0.55 m, approximately $1.3\%B$, in the original design. Thirty-one vertical ribs are uniformly arranged on each facade, and the spacing between two adjacent ribs is approximately 1.4 m, which is $B/30$.

2.2 Outline of the wind tunnel tests

The wind tunnel tests were conducted in the TJ-2 atmosphere boundary layer wind tunnel at the State Key Laboratory of Disaster Reduction in Civil Engineering, Tongji University. The size of its working section is $3.0m \times 2.5m$ ($width \times height$), and the working wind speed can be continuously adjusted up to 65 m/s.

The tested wind field was simulated as terrain category B in the Chinese structural load code(GB50009 2012), and its mean wind speed profile, turbulence intensity profile and PSD of wind speed are shown in Fig. 3. For the pressure measurement wind tunnel test, there were 350

pressure taps arranged on the tested models. The arrangement of the taps in the representative across section (at 2/3 of the building height) is shown in Fig. 2. The coordinates and the wind directions adopted in the present study are also included in Fig. 2. There are 40 wind directions in total for wind pressure tests, consisting of wind directions at every 10 degrees from 0° to 350° and 4 other wind directions: 45°, 135°, 225° and 315°. The length scale of the model is 1/300, and the blockage ratio of the wind tunnel is less than 5%. The tested wind speed atop the model is 9.02 m/s in all test cases. The actual building is located at a site with a basic wind pressure of 0.45 kN/m^2 for a 50-year return period, and the corresponding scales of wind speed and time are 1/4.7 and 1/63, respectively.

Fig. 1 Design sketch of the target building

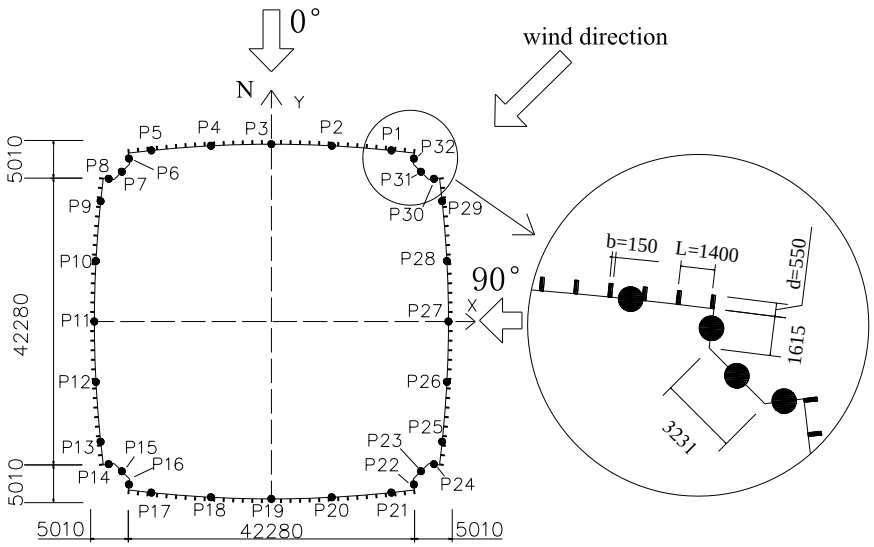

Fig. 2 Taps on cross section at 2/3 of the building height and definitions of wind angle and the coordinate

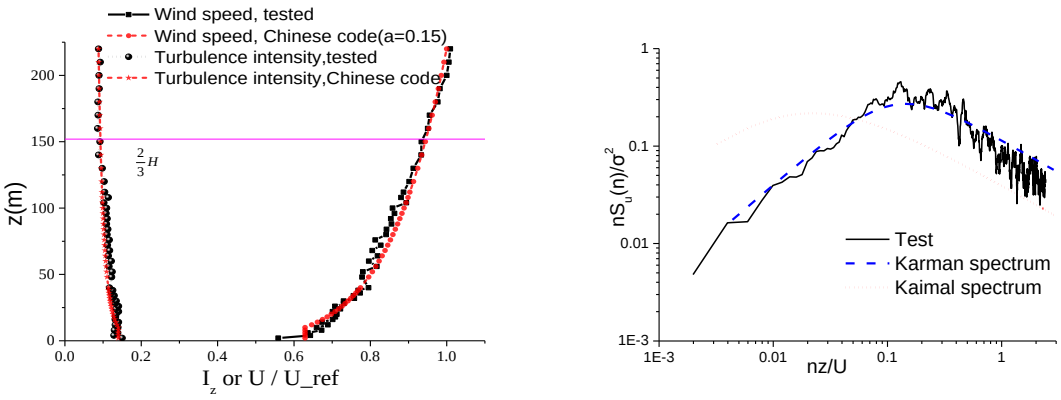

Fig. 3 Simulated mean wind speed profile, turbulence intensity profile and reduced power spectrum density of wind speed at the top of model

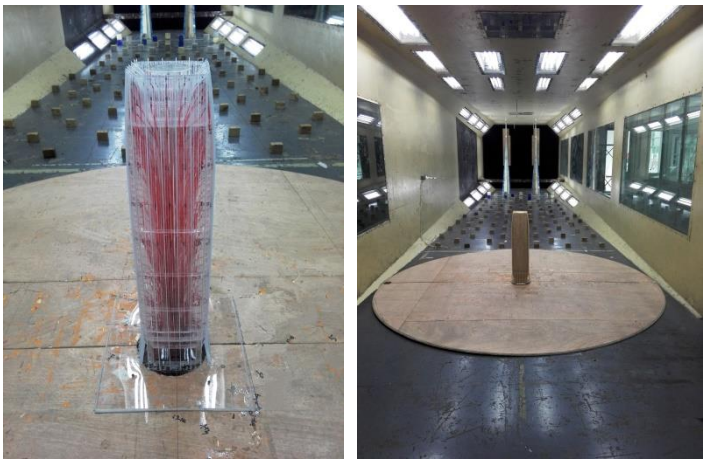

Fig. 4 Idealized wind tunnel test (wind pressure and HFFB) models

To obtain more widely applicable results, the surrounding buildings, canopy and podium of the actual building were removed from all the model cases in the present study, as shown in Fig. 4. A series of model cases with different rib spacing and depths were tested to analyze the effects of the depth and spacing of vertical ribs on the wind loads. Table 1 shows the tested model cases, in which S=s/B and D=d/B are the relative spacing and the relative depth of the ribs, respectively, and *s* and *d* are the spacing and depth of the ribs, respectively, as shown in Fig. 2. In Table 1, there are 8 models; Model 1 has no vertical ribs, and Model 2 is the original design of the actual building. Fig. 5 shows the schematic diagram of the vertical ribs on the facades of each model. Both the wind pressure measurement tests and high-frequency force balance tests in the wind tunnel were conducted for the 8 model cases, resulting in 16 total tested model cases.

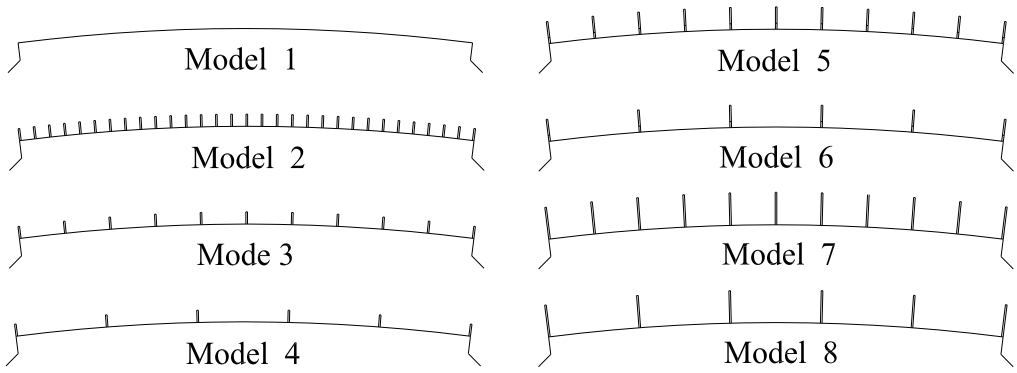

Fig. 5 Arrangement of ribs on one of the facades of each tested model case

Table 1 Model cases

Model Case	Model 1	Model 2	Model 3	Model 4	Model 5	Model 6	Model 7	Model 8
Relative Spacing(S)	1	1/30	1/10	1/5	1/10	1/5	1/10	1/5
Relative Depth(D)	0	1.3%	1.3%	1.3%	2.6%	2.6%	3.9%	3.9%

3. Data processing

The information of the wind pressure coefficients at the arranged taps was obtained through the wind pressure wind tunnel tests and the coefficients of the overall aerodynamic force (i.e., the base bending moments, shear forces and torques) were obtained from high-frequency force balance wind tunnel tests. The calculation process of wind pressure coefficients and aerodynamic force coefficients is introduced here.

3.1 Wind pressure coefficients

The wind pressure coefficients were calculated as follows

$$C_P(i,\theta,t)=\frac{P(i,\theta,t)}{0.5\rho U_H^2} \tag{1}$$

where $P(i,\theta,t)$ and $C_p(i,\theta,t)$ are the wind pressure and wind pressure coefficient at tap *i* for a wind angle of θ, respectively, ρ represents the air density with a value of 1.25 kg/m^3, U_H is the mean wind speed of the approaching wind on top of the building. C_{p_mean} and C_{p_rms} represent the mean and root mean square of the wind pressure coefficients, respectively.

The wind pressure coefficients do not follow Gaussian distributions. There are many studies on

calculating the extreme values of non-Gaussian pressure coefficients. Cook and Mayne (1980) proposed the Cook-Mayne coefficient with the goal of exceeding probability of structural wind pressures. Quan, Gu *et al*. (2009) proposed a method for extreme pressure coefficients using the extreme distribution type I based on observed time history data with a single standard observed period. Huang, Luo *et al*. (2016) recommended the Hermite polynomial model (HPM) to calculate the peak pressure coefficients due to its relatively high accuracy and efficiency for multiple wind pressure taps. In present study, Quan, Gu *et al*. (2009) proposed method and Cook-Mayne method (Cook and Mayne 1980) were combined to calculate the most unfavorable wind pressure coefficients for cladding/components design.

The most unfavorable wind pressure coefficients were calculated as follows

$$C_{P\_ext\_po}(i) = \max_{\theta=0\sim360}\left\{C_{P\_peak\_po}(i,\theta)\right\} \tag{2}$$

$$C_{P\_ext\_ne}(i) = \min_{\theta=0\sim360}\left\{C_{P\_peak\_ne}(i,\theta)\right\} \tag{3}$$

where $C_{p\_ext\_po}(i)$ and $C_{p\_ext\_ne}(i)$ are the most unfavorable positive and negative wind pressure coefficients (suction coefficients) at the tap of *i*, respectively. $C_{p\_peak\_po}(i,\theta)$ and $C_{p\_peak\_ne}(i,\theta)$ are the positive and negative extreme wind pressure coefficients at the tap of *i* and the wind direction of θ, which were calculated with Cook-Mayne method (Cook and Mayne 1980) as follows

$$C_{P\_peak} = \mu_{C_{p\_peak}} + 1.4/\alpha_{C_{p\_peak}} \tag{4}$$

where C_{p_peak} is the extreme value for a given measured tap and wind direction. $\mu_{C_{p\_peak}}$ and $\alpha_{C_{p\_peak}}$ are the mode and dispersion of the extreme distribution type I (the Gumbel distribution), respectively, which were calculated as follows (Quan, Gu *et al*. 2009)

$$\alpha_{C_{p\_peak}}(t_0) = \alpha_{C_{p\_peak}}(t_1) \tag{5}$$

$$\mu_{C_{p\_peak}}(t_0) = \mu_{C_{p\_peak}}(t_1) + \ln(t_0/t_1)/\alpha_{C_{p\_peak}} \tag{6}$$

where $\mu_{C_{p\_peak}}(t)$ and $\alpha_{C_{p\_peak}}(t)$ are the the mode and dispersion for observed period of *t*, respectively. t_0 and t_1 are the standard observed period and the observed period of sub-sections. The values $\mu_{C_{p\_peak}}$ and $\alpha_{C_{p\_peak}}$ used in Eq. (4) are for standard observed period, 10min. Quan *et al*. (2009) proposed an optimal observed period of sub-sections, t_1, with analyzing auto-correlation coefficients of time series of wind pressure coefficients. In present study, a standard sample was divided into 16 sub-sections with observed period of 37.5 sec. $\mu_{C_{p\_peak}}$ and $\alpha_{C_{p\_peak}}$ of sub-sections were calculated with moment method as follows (Holmes 2015)

$$\alpha_{C_{p\_peak}} = 1.28/\sigma_{\hat{C}_P} \tag{7}$$

$$\mu_{C_{p\_peak}} = U_{\hat{C}_P} - 0.45\sigma_{\hat{C}_P} \tag{8}$$

where $\sigma_{\hat{C}_p}$ and $U_{\hat{C}_p}$ are the standard deviation and mean values of the peak values of the 16 sub-sections with observing period of 37.5sec.

Eqs. (4)-(8) are applicable to the most unfavorable positive wind pressure coefficient. For the case of the most unfavorable negative wind pressure coefficient, the most unfavorable positive value of the opposite numbers of the wind pressure sample was calculated and then its opposite number was taken as the most unfavorable negative value.

3.2 Aerodynamic base force coefficients

Three components of aerodynamic base forces (*Qx*, *Qy* and *Qz*) and three components of aerodynamic base moments (*Mx*, *My* and *Mz*) were obtained from the high-frequency force balance wind tunnel tests. Due to the symmetry of the building, the aerodynamic base torsion (*Tz*) of a square high-rise building with corner recessions is small, and the four components of the aerodynamic force, *Qx*, *Qy*, *Mx* and *My*, have similar values. Only one of the aerodynamic base moments, *Mx*, was selected as the representative of the overall aerodynamic forces. The aerodynamic base moment coefficient was defined as

$$C_{Mx}(\theta,t)=\frac{Mx(\theta,t)}{0.5\rho U_H^2 B_a H^2} \tag{9}$$

where H is the height of the building and B_a is the average feature breadth. There are varying breadths for different floors; thus, the average feature breadth was adopted

$$B_a=\frac{1}{H}\sum_{i=1}^{N}h_i B_i \tag{10}$$

where h_i and B_i are the height and breadth of the building at the i^{th} floor, respectively, and N is the number of floors.

Additionally, the mean and RMS values of the aerodynamic base moment coefficient, C_{Mx}, are represented by C_{Mx_mean} and C_{Mx_rms}, respectively.

The reduced power spectrum of the aerodynamic base moment coefficient was expressed as follows:

$$S_{Mx}^{*}(\theta,f)=\frac{fS_{Mx}(\theta,f)}{(0.5\rho U_H^2 B_a H^2)^2} \tag{11}$$

where S_{Mx} is the power spectrum of the aerodynamic base moment, *Mx*.

4. Results of the wind pressure coefficients

The statistic values of wind pressure coefficients at each tap on the tested models were calculated using Eqs. (1)-(8). The wind pressure coefficients are analyzed in the following sections according to three aspects including a wind direction of 0°, the effects of wind direction and the most unfavorable values.

4.1 Wind direction of 0°

The test case for a wind direction of 0° is a typical case in which the wind blows toward the structural axis. The mean and RMS values of the wind pressure coefficients are discussed in the following.

4.1.1 Mean wind pressure coefficients

Figs. 6 and 7 show the contours of the mean wind pressure coefficients of Model 1 (the model case without ribs) and Model 8 (the model case with the deepest ribs spaced the farthest apart, D=3.9% and S= 1/5) for the wind direction of 0°.

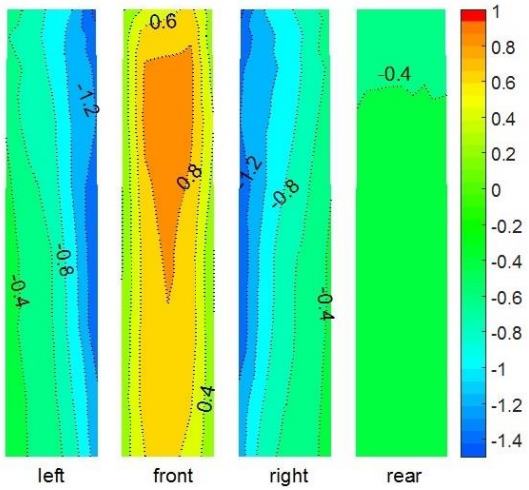

Fig. 6 Contours of C_{p_mean} of Model 1 (without ribs) for wind angle of 0°

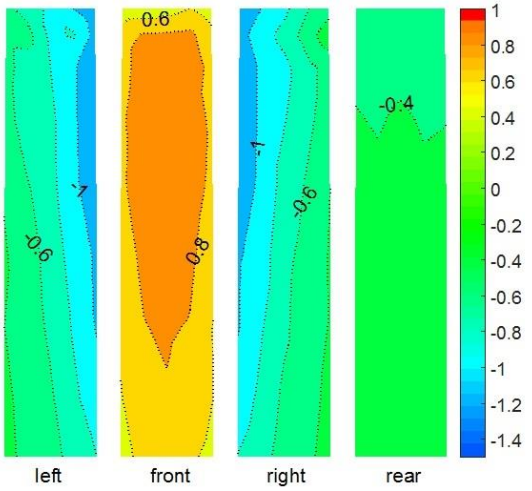

Fig. 7 Contours of C_{p_mean} of Model 8 (S=1/5 and D=3.9%) for wind angle of 0°

On the windward facade, the maximum value of C_{p_mean} for Model 1 is approximately 0.93, which appears in the middle region near 2/3 of the building height; however, the range encompassed by the 0.8 contour line is small. The contour lines of C_{p_mean} are dense except on the lower part. From the middle region to the outward edge regions, C_{p_mean} decays rapidly so that C_{p_mean} is less than 0.4 near the edge. However, for Model 8, even though the maximum value of C_{p_mean}, 0.96, is not considerably larger than the corresponding value of Model 1, the range encompassed by the 0.8 contour line increased significantly, and the C_{p_mean} contour lines became more spread out. From the middle region to the edge regions, C_{p_mean} decays slowly. The values of C_{p_mean} near the edge are between 0.6 and 0.8, which are notably higher than the corresponding values of the smooth model case (Model 1).

On the sideward facades, the maximum suction coefficients ($-C_{p\_mean}$) are mostly over 1.2 for Model 1 at the windward edge regions. The suction coefficients gradually decrease from a high value in the windward edge regions to a low value of less than 0.4 in the leeward edge regions. For Model 8, although the wind pressure distributions are similar to those of Model 1, the maximum suction coefficients in the windward edge regions are below 1.2 and even below 1.0 at some taps. The suction coefficients in the leeward edge regions increase to over 0.4. These conditions show that the ribs can weaken the high suction coefficients in the windward edge regions but slightly increase the lower suction coefficients in the leeward edge regions.

The C_{p_mean} values on the leeward facade are uniform and are approximately -0.4. There are no obvious differences between Model 1 and Model 8.

The C_{p_mean} values in the corner recession regions are difficult to represent in the contour maps because there are only a few measured taps there. To make the results more comprehensive, the C_{p_mean} values on the cross section at 2/3 of the building height are analyzed here.

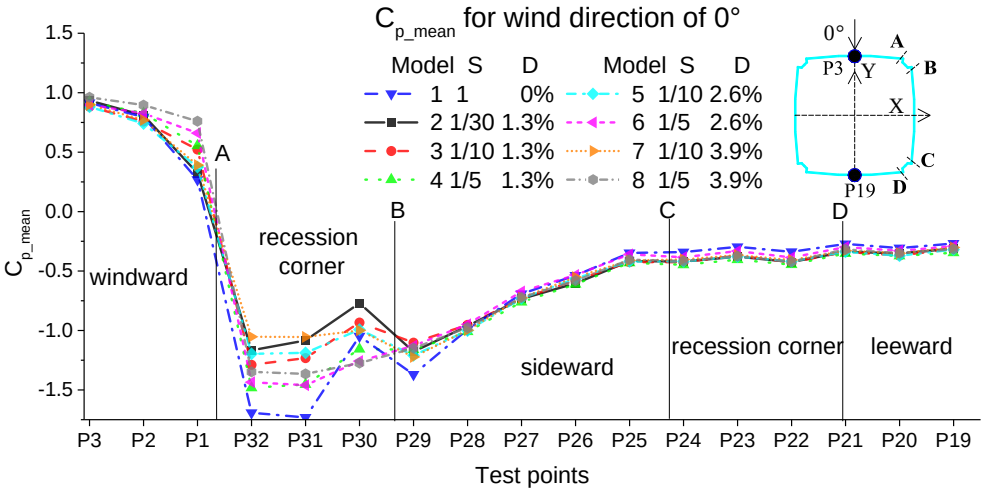

Fig. 8 C_{p_mean} of taps on the cross section at 2/3 of the building height for wind angle of 0°

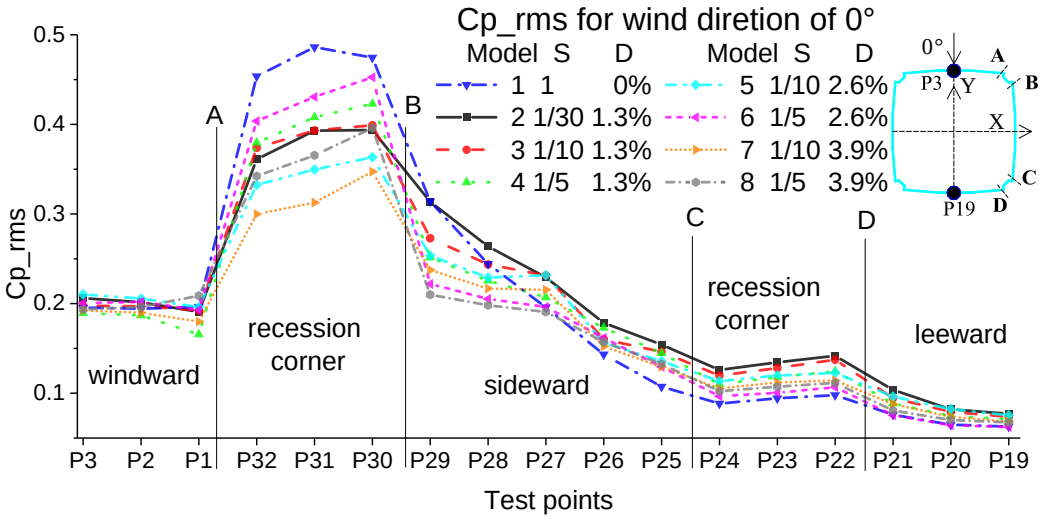

Fig. 9 C_{p_rms} of taps on the cross section at 2/3 of the building height for wind angle of 0°

Fig. 8 shows the values of C_{p_mean} at the taps on the cross section at 2/3 of the building height in the wind direction of 0°. Because the building shape and wind direction are symmetrical along the Y axis, only the data on the right side of the Y axis are given. The horizontal coordinates are the serial numbers of the measured taps, as shown in Fig. 2.

At tap P3 in the middle region of the windward facade, the C_{p_mean} values of all the model cases are 0.88~0.96, the maximum values of all the taps in this cross section, and the variability among model cases are very small. At tap P1 in the edge regions of the windward facade, the distinctions of C_{p_mean} among model cases are significantly increased; C_{p_mean} at tap P1 on Model 1 is +0.25, which is the minimum of all the model cases and is only 27% of the corresponding value at tap P3 in the center region. The deeper or more spread out the ribs are, the larger C_{p_mean} will be. C_{p_mean} at tap P1 on Model 8 (the model with the deepest and most spread out ribs) is +0.75, which is the maximum value among all the model cases and is approximately 3 times larger than the corresponding value on Model 1.

The effects of ribs on the mean wind pressure coefficients at the windward corner recession regions (P32, P31 and P30) are very obvious. The suction coefficients ($-C_{p\_mean}$) at taps P32 and P31 are very large for Model 1 at 1.69 and 1.73, respectively. For the model cases with ribs, the suction coefficients at taps P32 and P31 are significantly weakened, and the deeper or denser the ribs are, the weaker the suction coefficients will be. The suction coefficients at taps P32 and P31 decrease to 1.05 for Model 7, which has the deepest and the closest ribs. This value is 60% of the corresponding value for Model 1.

The suction coefficients at tap P30 are smaller than the values at taps P32 and P31. The C_{p_mean} of Model 1 is approximately -1.05; relatively dense ribs weaken the suction coefficients, while ribs spaced farther apart (S=1/5) will strengthen the suction coefficients.

On the sideward facades, the pressure coefficients are obviously affected by the ribs only on the taps in the windward edge regions (tap P29). At tap P29, the suction coefficient of Model 1 is 1.37, which is the largest value; the suction coefficients of the model cases with ribs are 1.1~1.2.

On the leeward region of the sideward facades, leeward facade and the leeward recession corner region, C_{p_mean} has relatively small values.

Overall, when the wind is flowing toward one facade, the ribs have no significant effects on C_{p_mean} in the middle region of the windward facade, but the ribs enlarge the low pressure coefficients in the edge region. The deeper or farther apart the ribs are, the stronger the enlargement effects are. In the windward corner recession regions and the windward edge regions of the sideward facades, the ribs decrease the high suction coefficients; this effect is stronger for deeper or denser ribs. On the leeward regions of the sideward facades, leeward facade and the leeward corner recession regions, the effects of ribs on the low suction coefficients are not obvious.

For Model 1, whose surface is smooth, air freely blows tangentially along the windward facade and the free-flow is separated from the corner edge, which forms periodic vortex shedding blowing to the wake region. Therefore, the wind pressures in the central region of the windward facade are high, while low values appear in the region far from the middle. High suction coefficients appear in the windward corner recession regions and windward edge regions of the sideward facades, while low suction coefficients appear in the leeward edge regions of the sideward facades, leeward corner recession regions and leeward facade. In the model cases with vertical ribs, the ribs block the airflow blowing tangentially along the windward facade and impede the gradual weakening of the high wind pressures from the middle region to the edge regions, increasing the low wind pressures in the edge regions of the windward facade and making the wind pressures on the windward facade more uniform. The vortices on both sides of the building make the airflow blow tangentially along the sideward facades, and the vertical ribs on the sideward facades block these tangential flows suppressing the vortices and greatly reducing the high suction coefficients in the windward edge regions of the sideward facades induced by the vortex.

4.1.2 RMS of the wind pressure coefficients

Fig. 9 illustrates the variations of C_{p_rms} versus position on the cross section of at 2/3 of the building height at the wind angle of 0°.

At tap P3 in the middle region of the windward facade, the C_{p_rms} values of all the model cases are 0.2, which is very small. From the middle to the edge, the change in C_{p_rms} is not obvious. The influence of the ribs on C_{p_rms} is also not significant.

In the windward corner recession region (Taps P32, P31 and P30), the C_{p_rms} values are very high for all the model cases. The values on the smooth model case (Model 1) are the maximum values among all the tested model cases; the value at tap P31 reaches 0.49. For most of the model cases with ribs, the C_{p_rms} values gradually increase from tap P32 to tap P30 and reach a maximum value at tap P30. The deeper and denser ribs decrease the C_{p_rms} values more effectively. The C_{p_rms} value of Model 7 (with the deepest and densest ribs) is approximately 0.31 at tap P31, which decreases 63% from that of Model 1.

The C_{p_rms} values on the sideward facades of all the model cases greatly decrease from the corresponding values in the windward corner recession regions. In the windward edge regions of the sideward facades, the values of C_{p_rms} on Model 1 and Model 2 (the model case with densest ribs) are both approximately 0.31. With decreasing rib density or increasing rib depth, the C_{p_rms} gradually decreases. The C_{p_rms} value of Model 8 (the model case with the deepest and most widely spaced ribs) decrease to 0.21, which is about 65% of the corresponding value for the smooth model case.

On the sideward facades, the C_{p_rms} values decrease rapidly from the windward edge region (tap P29) to the leeward edge region (tap P25). In this process, the C_{p_rms} values of Model 1 decrease most rapidly, and the value at tap P25 in the leeward edge region is only approximately 0.06. From the middle region (tap P27) of the sideward facades to the leeward facade (taps P21, P20 and P19), the C_{p_rms} values of Model 1 (without ribs) are the smallest of all the tested model cases.

Overall, the ribs have little effect on C_{p_rms} on the windward facade but can significantly suppress the high values of C_{p_rms} in the windward corner recession regions and the windward edge regions of the sideward facades. In addition, the deeper and closer ribs have a better suppressing effect. In the leeward regions of the sideward facades, leeward corner recession regions and leeward facade, the ribs seem to enlarge the low values of C_{p_rms}.

As mentioned above, vertical ribs block the airflow blowing tangentially along the sideward facades, suppressing the vortex shedding and therefore decreasing the high C_{p_rms} values in the windward corner recession regions and the windward edge regions of sideward facades. In the leeward region of the sideward facades, leeward corner recession regions and leeward facade (the region from P27 to P19), small vortices are induced by the ribs, increasing the C_{p_rms} in these regions. On the windward facade, the ribs mainly hinder the wind flowing along the facade and C_{p_rms} is mainly induced by the turbulence of the incoming flow; thus, the ribs have little effect on C_{p_rms} on the windward facade.

4.2 The effects of wind direction

The influence of ribs on the wind pressure distributions on the facades at the wind angle of 0° is analyzed above. Three representative taps (P32, P1 and P3, as shown in Fig. 2) on the cross section at 2/3 of the building height are selected to further analyze the effects of ribs on wind pressure under various wind directions. Taps P32, P1 and P3 represent the taps in the corner recession region, the edge region of the facades and the middle region of the facades, respectively.

4.2.1 Mean values

Fig. 10 shows the C_{p_mean} values at tap P32 versus wind angle. When the wind angle is near 0° (including 350°), the airflow blows from the north to south and separates from the two edges of the north facade (Fig. 2).

Tap P32 is located at the downstream region, where the peak suction coefficients appear. The model case without ribs has the maximum suction coefficients of 1.6 among all the tested model cases. The maximum suction coefficient of Model 6 (D=2.6%, S=1/5) is suppressed the most by the ribs and is about 75% of the corresponding value of Model 1 (without ribs). When the wind angle is near 90° (including 100°), the airflow blows from east to west and separates from the two edges of the east facade. Tap P32 is located at the downstream region, where the peak value of C_{p_mean} appears once more. However, the peak values of suction coefficients are smaller than that for the wind angle near 0° because tap P32 is farther away from the point of separation in this case. When the wind angle is near 45°, the airflow blows from northeast to southwest, facing the corner recession region where P32 is located. The values of C_{p_mean} for all of the model cases approach the maximum value of 0.9 at tap P32, and there are no significant differences among the tested model cases.

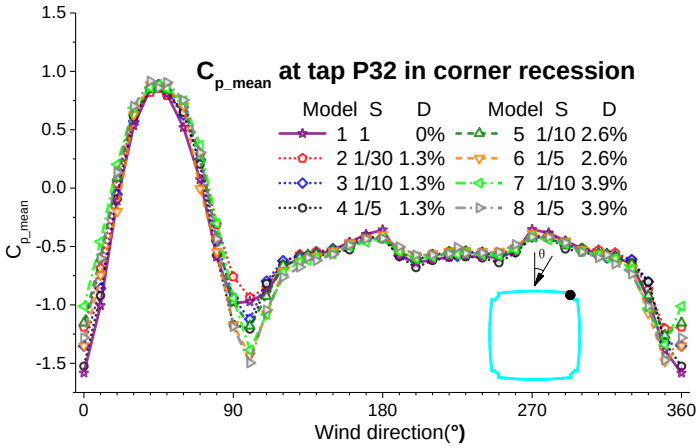

Fig. 10 C_{p_mean} at tap P32 versus wind angle

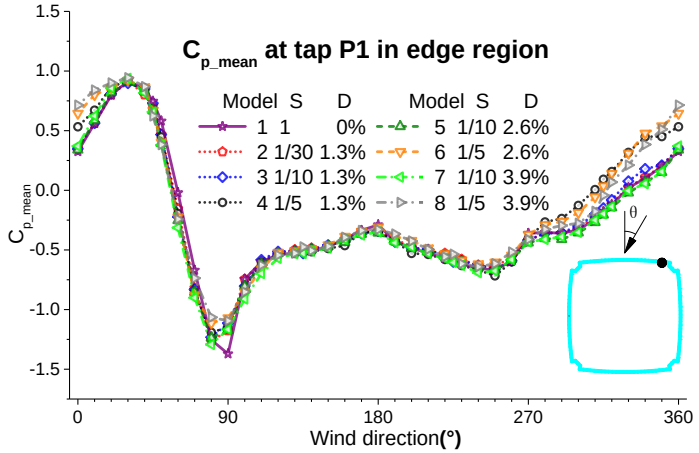

Fig. 11 C_{p_mean} at tap P1 versus wind angle

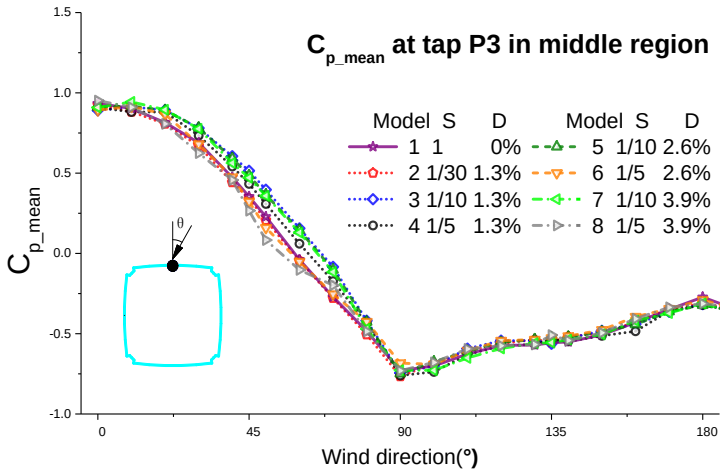

Fig. 12 $C_{\text{p\_mean}}$ at tap P3 versus wind angle

Fig. 11 shows C_{p_mean} at tap P1 versus wind direction angle. In general, the variations for each model case are similar. At the wind angle of 0°, the C_{p_mean} value of Model 1 (without ribs) is 0.32, which is smaller than those of the model cases with ribs, which vary between 0.34 and 0.71. With increasing wind angle, C_{p_mean} of all the model cases increase, and the differences between them gradually decrease. At the wind angle of 30°, the C_{p_mean} values of all the model cases at tap P1 reach the maximum value of approximately 0.9, and the differences among tested model cases are very small. Then, the C_{p_mean} values of all the model cases gradually decrease with increasing wind angle up to 90°. At this wind angle, the airflow separates from two edges of the east facade; P1 is located at the separated flow region, where the maximum suction values appear. C_{p_mean} of Model 1 (without ribs) is approximately -1.4 at this wind angle. As described above, vertical ribs suppress vortex shedding, making the suction coefficients of the model cases with ribs smaller than the corresponding values of the model without ribs. The minimum suction coefficient of the model cases with ribs at the wind angle of 90° is -1.07, which is approximately 75% of the corresponding value for the model case without ribs.

Fig. 12 shows C_{p_mean} at tap P3 versus wind direction angle. As the building shape is symmetrical and tap P3 is located on the symmetric axis, the information for the wind angles of 0°-180° are the same as that for the wind angles of 180°-360°; therefore, only the values for wind angles of 0°-180° are analyzed here.

When the wind direction angle is 0 degrees, tap P3 is located at the stagnation point of the windward facade, and the C_{p_mean} values at tap P3 of all the tested model cases reach their maximum values of approximately 0.9. As the wind angle increases up to 90°, the C_{p_mean} gradually decreases to its negative peak of approximately -0.75 at the wind angle of 90°. When the wind angle increases from 90° to 180°, the suction coefficients gradually decrease. At a 180° wind angle, the C_{p_mean} values are only 1/3 of the corresponding values at the wind angle of 90°.

Overall, the ribs have few effects on C_{p_mean} in the middle region. The ribs have only some influence when the wind angle is between 30° and 70°; because the ribs block the airflow flowing tangentially along the facade, they mainly increase C_{p_mean}.

4.2.2 Fluctuating values

Fig. 13 shows C_{p_rms} at tap P32 versus wind direction angle. Near the wind angles of 0° and 90°, where P32 is in a separated wake, the C_{p_rms} values of tap P32 on all tested model cases show peaks, and the differences among the model cases are relatively very large. The model case with the maximum C_{p_rms} of 0.45 is still Model 1 (without ribs). The ribs can suppress the high C_{p_rms} in the windward corner recession region, and deeper and closer ribs have better suppressing effects. The maximum C_{p_rms} of Model 7 (D=3.9% and S=1/10) is only 2/3 of the corresponding value of Model 1 (without ribs) because the ribs suppress vortex shedding. At the wind angles far from 0° and 90°, the C_{p_rms} values are smaller and not sensitive to the ribs.

Fig. 14 shows the C_{p_rms} at tap P1 in the edge region of the facade versus wind direction angle. When the wind angle increases from 0° to 40°, the variation of C_{p_rms} is not large at approximately 0.2. As the wind angle increases from 40° to 60°, C_{p_rms} increases rapidly. At the wind angle of 60°, the C_{p_rms} of each model increases to approximately 0.3. Then, with increasing wind angle, the C_{p_rms} of Model 1 continuously increases and reaches its peak value of 0.34 at the 90° wind angle. However, at the wind angle near 90°, the C_{p_rms} values of the model cases with ribs fall within a larger range. With increasing rib density and depth, the C_{p_rms} gradually decreases. The minimum value of all tested model cases is for Model 8 (with the largest rib spacing and depth); this value is only 60% of the corresponding value for Model 1 (without ribs). These phenomena again indicate that ribs suppress vortex shedding.

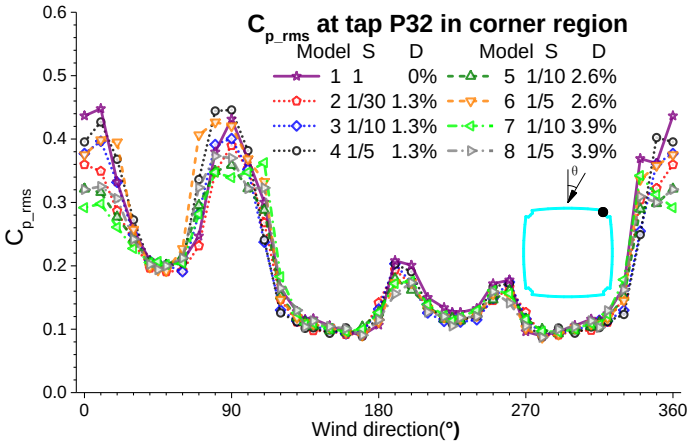

Fig. 13 C_{p_rms} at tap P32 versus wind angle

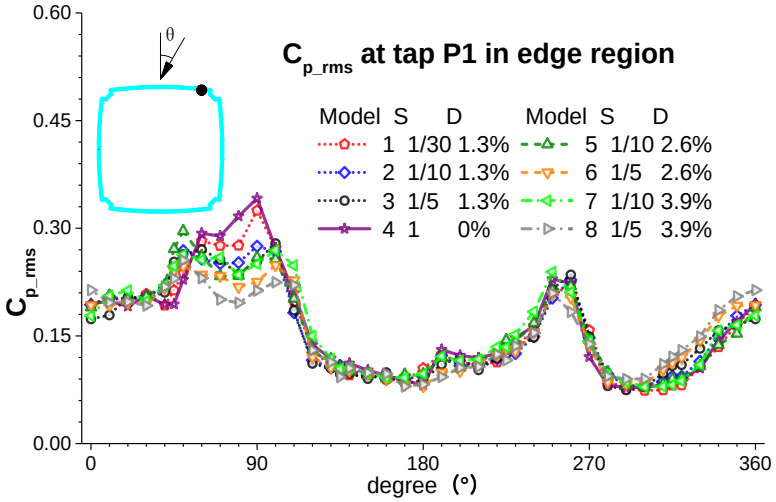

Fig. 14 C_{p_rms} at tap P1 versus wind angle

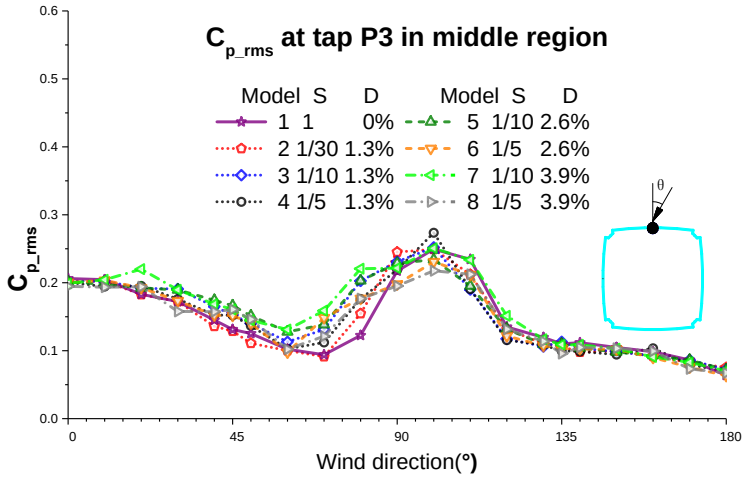

Fig. 15 C_{p_rms} at tap P3 versus wind angle

The C_{p_rms} at tap P3 versus wind direction angle is shown as Fig. 15. All the C_{p_rms} are relatively small values at below 0.3. The maximum value appears at the wind angle of 90°, where tap P3 is located at the middle of the sideward facade, and the change trend in this region is also relatively messy.

4.3 The most unfavorable wind pressure coefficients

The most unfavorable wind pressure coefficients are often chosen for the design wind loads of components or cladding of buildings.

4.3.1 The most unfavorable negative pressure coefficients

Fig. 16 shows the most unfavorable negative coefficients ($C_{p\_ext\_ne}$) at tap P32 in the corner recession regions. The most unfavorable suction coefficients ($-C_{p\_ext\_ne}$) of Model 1 (without ribs) is the largest one of all the tested model cases and the value is 3.4 approximately. The most unfavorable suction coefficients of the model cases with ribs are diminished by the ribs; these values are 2.6~3.1, which are 76%~91% of the corresponding value of Model 1. The denser ribs with the same depth have more powerful suppression effects on the most unfavorable suction coefficients. For the same rib density, when the depth of the ribs increase, the most unfavorable suction coefficients mainly decrease.

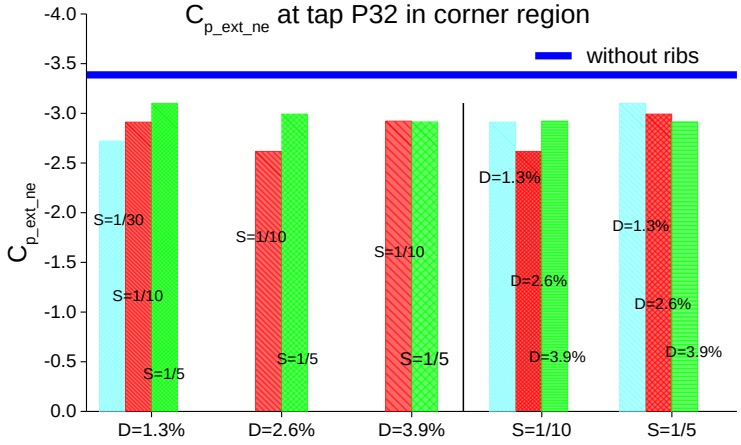

Fig. 16 $C_{p\_ext\_ne}$ at tap P32 in the recession corner region of the facade

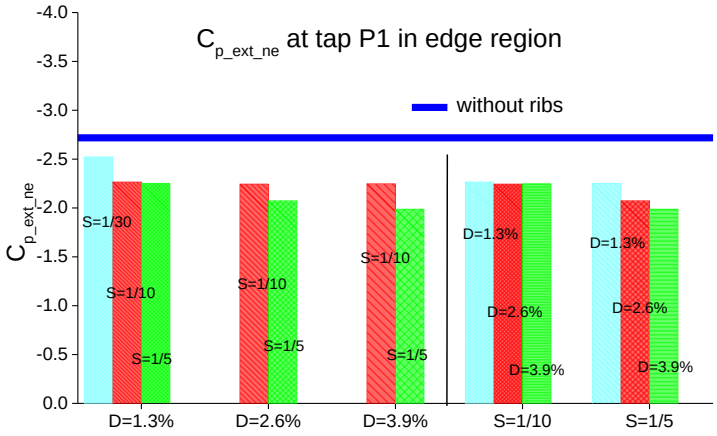

Fig. 17 $C_{p\_ext\_ne}$ at tap P1 in the edge region of the facade

Fig. 17 shows the $C_{p\_ext\_ne}$ values at tap P1 in the edge region of the facade. The most unfavorable suction coefficient of Model 1 (without ribs) is the largest value of 2.7. The most unfavorable suction coefficients at this region of the tested model cases with ribs are also suppressed by the ribs; their values decrease to 2.0~2.5, which are 74%~93% of the corresponding value for Model 1. Farther apart ribs with same depth have more powerful suppression effects on the most unfavorable suction coefficients. When the spacing is the same, the rib depth has no obvious effect on the most unfavorable suction coefficients.

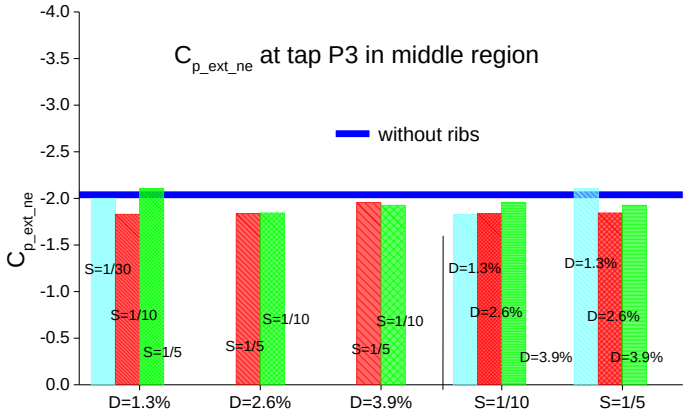

Fig. 18 $C_{p\_ext\_ne}$ at tap P3 in the middle region of the facade

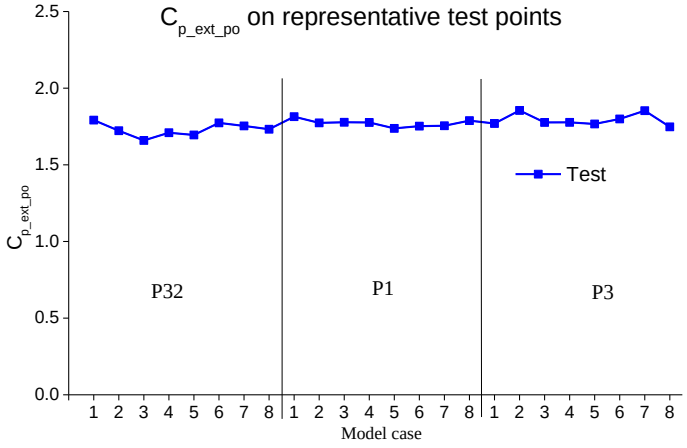

Fig. 19 Test results of $C_{p\_ext\_po}$ at representative taps

Fig. 18 shows the $C_{p\_ext\_ne}$ values at tap P3 in the middle region of the facade. The most unfavorable suction coefficient of this region is relatively small and only approximately 60% of the corresponding value in the corner regions. The influence of the ribs on the most unfavorable suction coefficient is small and does not have obvious regularity. Sometimes, the ribs slightly increase the suction coefficients. Overall, the most unfavorable suction coefficients in the middle region are not obviously affected by the ribs, and they are much smaller than those in the edge regions and the corner recession regions; therefore, they are not critical for the structural design of buildings.

4.3.2 The most unfavorable positive pressure coefficients

Fig. 19 shows the most unfavorable positive pressure coefficients, $C_{p\_ext\_po}$, of all the tested model cases at three representative taps (P32, P1 and P3). The $C_{p\_ext\_po}$ values of all the model cases at these three taps are approximately 1.75, and the effects of the rib and tap positions on $C_{p\_ext\_po}$ are very small.

Even though the above results are mainly based on the test data at 2/3 height, the test results show that there are similar regularities at other heights except that the wind pressure coefficients near the top and bottom of the building are significantly affected by the three-dimensional flow effect.

5. Results of the aerodynamic forces

As mentioned above, only the aerodynamic base moments in the X direction are discussed here.

5.1 Mean aerodynamic force coefficients

Fig. 20 shows the variations of C_{Mx_mean} versus wind direction angle. When the wind angle increases from 0° to 30°, the C_{Mx_mean} values of all the tested model cases increase gradually. From 30° to 90°, C_{Mx_mean} values gradually decay. Although the trends of C_{Mx_mean} are similar, the values of different model cases differ at the same wind angle. The values of C_{Mx_mean} for Model 1 (without ribs) are basically the smallest among all the tested model cases. The most unfavorable condition is the 30° wind angle because of the corner recession.

Fig. 21 shows the values of C_{Mx_mean} at a wind angle of 30°. The figure indicates that the vertical ribs increase C_{Mx_mean} for most model cases, but the degree of increase varies widely for different ribs. For most models, the farther apart the ribs are (larger D), the larger C_{Mx_mean} will be. When the relative spacing is 1/5 and the relative depth is 1.3% (Model 4), C_{Mx_mean} has the largest value of approximately 0.5, which is 10% larger than the value of Model 1 (without ribs). When the relative spacing decreases to 1/10, vertical ribs with different depths have varying enlarging effects on C_{Mx_mean}. As the relative spacing decreases to 1/30, the ribs will slightly decrease C_{Mx_mean}.

The case with the wind angle of 0° is a typical case, and the aerodynamic force coefficients in

this case are often used to determine the design wind loads for buildings. Fig. 22 shows the C_{Mx_mean} of each model at this wind angle. When the relative depth is 2.6% and the relative spacing is 1/10, C_{Mx_mean} is the maximum value among all the tested model cases and is 30% larger than the value of Model 1 (without ribs). Among all the tested model cases, the C_{Mx_mean} value of Model 4 (D =1.3% and S = 1/30) has the smallest increment of approximately 10% from the corresponding value of Model 1 (without ribs).

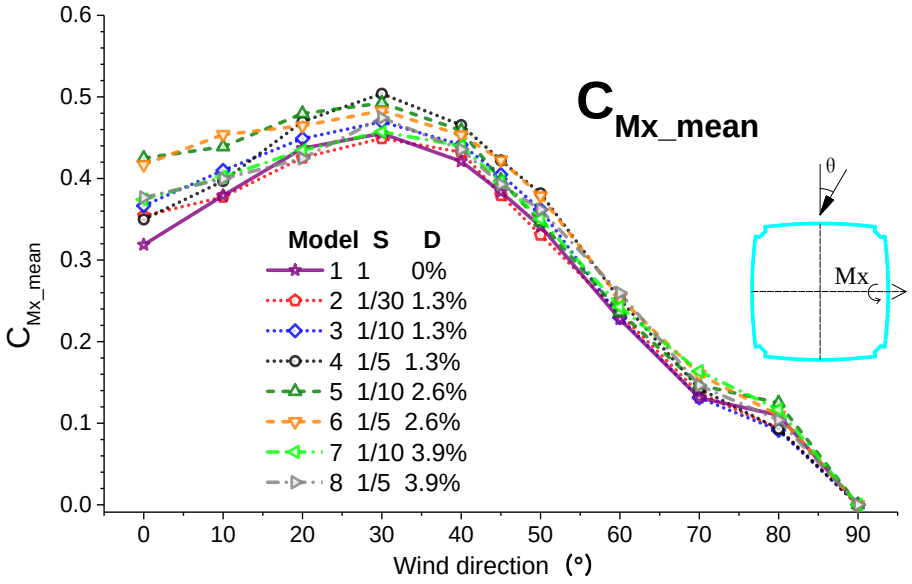

Fig. 20 C_{Mx_mean} versus wind angles

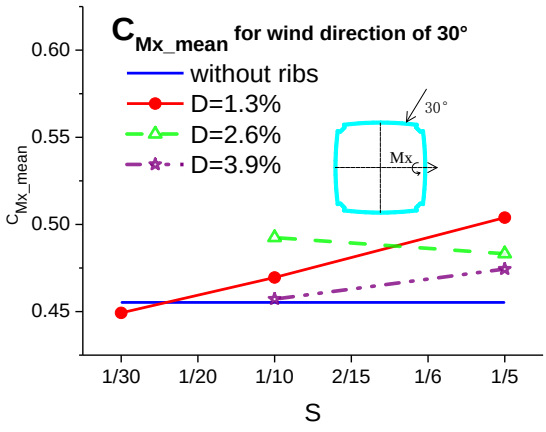

Fig. 21 Effects of ribs on C_{Mx_mean} at a wind angle of 30°

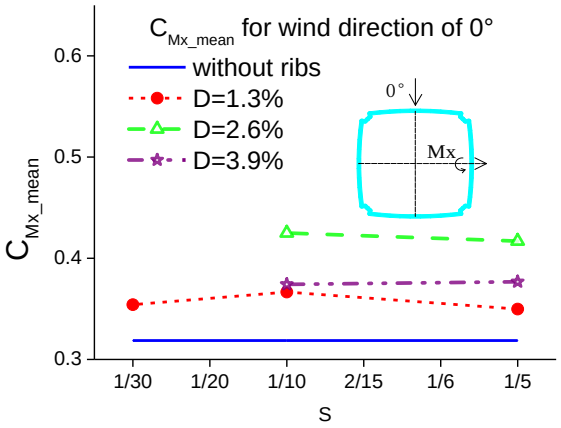

Fig. 22 Effects of ribs on C_{Mx_mean} at wind angle of 0°

For Model 1 (without ribs) at the wind angle of 30°, considerable airflow blows tangentially along the east facade (as shown in Fig. 2) from north to south, and part of the airflow blows tangentially along the north facade from east to west, so that the wind pressure coefficients in the northeast corner recession region (taps P32, P31 and P30) and the windward region of the north facade (close to taps P1 and P2) show high positive values (Fig. 10 and Fig. 11); therefore, C_{Mx_mean} reaches its maximum value at this wind angle.

When vertical ribs appear, the ribs on the east facade block the airflow flowing tangentially along the east facade from north to south so that the ribs on the east facade obtain the aerodynamic forces in the reverse *Y* direction, enlarging the base moments in the *X* direction. At the same time, the ribs on the north facade block the airflow flowing tangentially along the north facade from east to west, so that the relatively low pressure coefficients in the middle region (tap P3 in Fig. 12) and the leeward region (tap P4 and P5, corresponding to tap P1 in Fig. 11 at 330°) on the north facade increase significantly close to the high pressure (taps P1 and P3 at Fig. 11 and Fig. 12) in the windward region (near P1 and P2); therefore, the base moment coefficients in the *X* direction increase.

When the wind direction angle is 0°, the airflow blows tangentially along both the east and west sideward facades from north to south. However, the ribs on the sideward facades block the tangential flow, resulting in additional aerodynamic forces in the inverse *Y* direction. In addition, the ribs of the north windward facade increase the positive wind pressure near the edge region of this facade, resulting in getting additional aerodynamic forces in the inverse *Y* direction on the north facade. These two factors increase the base moment coefficients in the *X* direction.

5.2 Fluctuating aerodynamic force coefficients

Fig. 23 shows the variations of C_{Mx_rms} versus wind direction angle. At the wind direction angle of 0°, C_{Mx_rms} is caused by the along-wind aerodynamic force. The C_{Mx_rms} of Model 1 (without ribs) has a small value of 0.054. The smallest C_{Mx_rms} of all the tested model cases,

which is 0.052 and approximately 5% of that of Model 1, are for Model 4 and Model 8, which both have the maximum relative spacing (1/5). The C_{Mx_rms} of Model 5 (S =1/10 and D =2.6%) has the largest value at over 40% larger than the value of Model 1 (without ribs).

At the wind direction angle of 90°, *Mx* is caused by the across-wind aerodynamic force. The C_{Mx_rms} values of all the tested model cases are between 0.065 and 0.077, which are relatively large. The influence of the ribs is not the same: ribs increase C_{Mx_rms} in some model cases and decrease them in other cases. The influence range mostly falls within 10%.

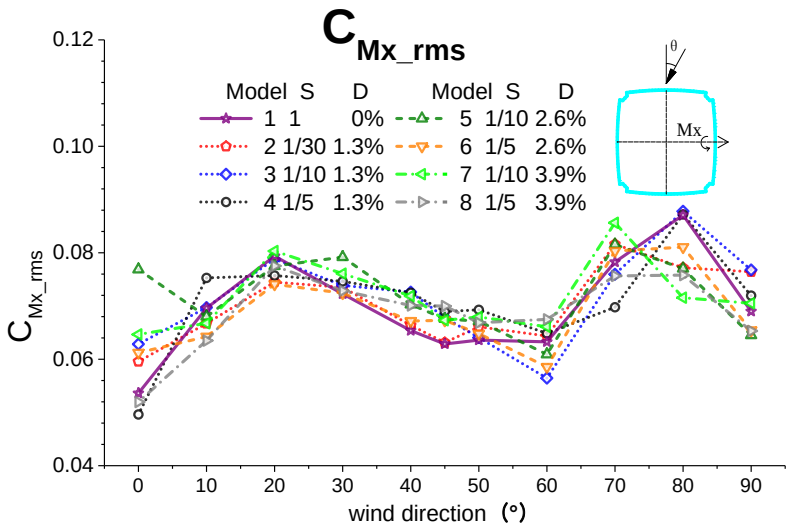

Fig. 23 C_{Mx_rms} versus wind angle

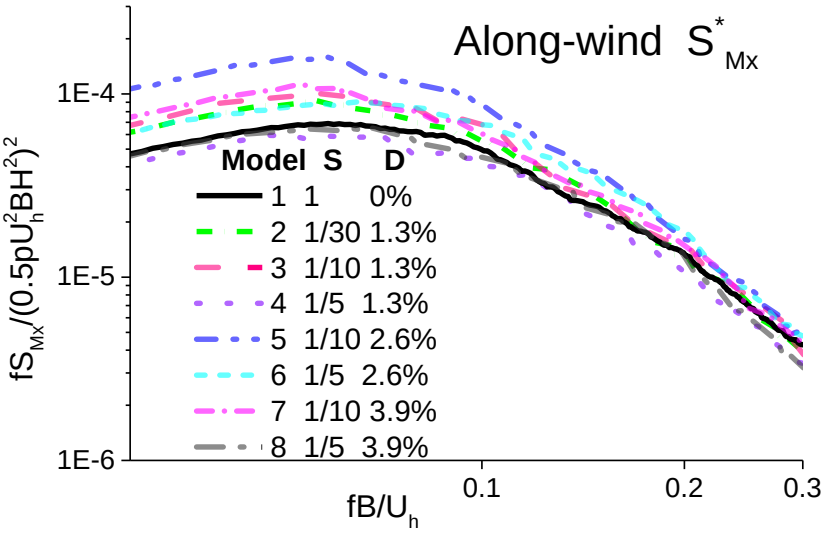

Fig. 24 Normalized PSD of along-wind base moment coefficients

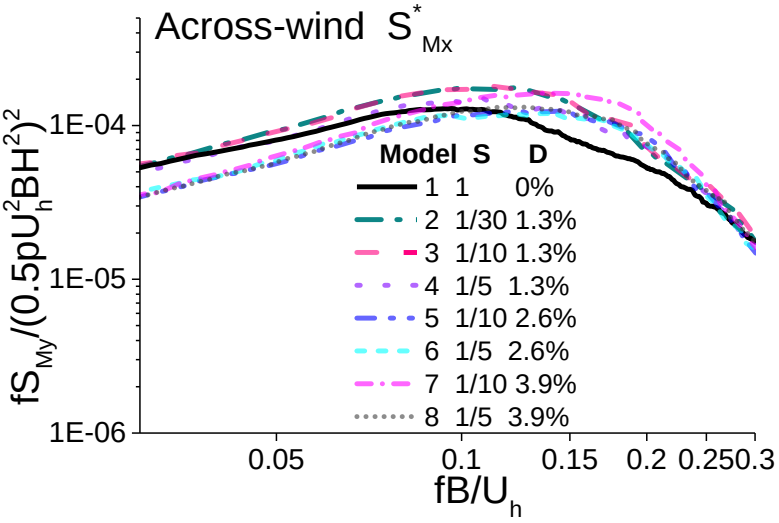

Fig. 25 Normalized PSD of across-wind base moment coefficients

Fig. 24 shows the normalized power spectrum, S^*_{Mx}, calculated from Eq. (11), of *Mx* at the wind angle of 0°. The *Mx* is caused by the along-wind aerodynamics at this wind angle. The S^*_{Mx} of all model cases are broadband spectra, and there are no significant peaks. For a reduced frequency of greater than 0.2, the spectra of all model cases are relatively low, and there are no obvious differences among the different model cases; therefore, the ribs have no obvious effects on the high-frequency region of the reduced power spectra of the along-wind aerodynamic forces. When the reduced frequency is less than 0.1, except for Model 4 and Model 8, the energy of S^*_{Mx} for the other tested model cases are obviously higher than this value for Model 1 (without ribs). This result is consistent with the results shown in Fig. 23.

As shown in Fig. 9, the ribs have almost no effect on the fluctuating wind pressures on the windward facade but have some suppression effect on the fluctuating wind pressures in the windward corner recession region, slightly decreasing the along-wind aerodynamic force. However, the ribs increase the fluctuating wind pressure on the leeward facade and leeward corner recession region. In addition, the ribs on the sideward facades can obtain fluctuating aerodynamic forces in the -Y direction. Therefore, the along-wind fluctuating aerodynamic forces increase. Overall, the ribs increase the along-wind fluctuating aerodynamic force.

Fig. 25 illustrates the normalized power spectrum (S^*_{Mx}) of *Mx* at a wind angle of 90°. *Mx* is caused by the across-wind aerodynamic forces at this wind direction. Due to the effects of corner recession on the wind pressure, the Strouhal peak of S^*_{Mx} is not prominent (Gu and Quan 2004).

The S^*_{Mx} of Model 1 (without ribs) has its peak value at the reduced frequency of 0.11. After adding the ribs, the reduced frequency of the peak value increase.

The S^*_{Mx} for the model case with ribs at the high-frequency region (0.15~0.20) increased from those of Model 1 (without ribs).

For Model 1 (without ribs), as the airflow blows from east to west, there are very large fluctuating wind pressures at the windward edge regions of the sideward facades (such as at tap P1, as shown in Fig. 2) resulting from vortex shedding. However, the fluctuating wind pressure greatly decrease at the leeward edge of the sideward facades (such as at P5). For the model cases with ribs, the high fluctuating wind pressures at the windward edge region of the sideward facades (such as at tap P1) are weakened because the vortex shedding from the windward edges is disturbed by the ribs. At the same time, the low fluctuating wind pressures in the leeward edge regions of the sideward facades (such as at P27) and leeward facade significantly increase (as shown in Fig. 9) because small vortices are induced by the ribs in these region; therefore, the ribs sometimes weaken the fluctuating aerodynamic force coefficients and sometimes increase them. Naudascher, Weske *et al*. (1981) noted that ribs will disrupt the across-wind vortex shedding, which decreases the peak of the power spectrum. In the present case, in which there are corner recessions and ribs on the studied building, the ribs do not always reduce the across-wind fluctuating aerodynamic forces because the ribs suppress large vortex shedding at both sides of the building and simultaneously induce small vortices behind the ribs downstream.

Overall, the vertical ribs increase the along-wind fluctuating aerodynamic forces in most cases but have no obvious regular effects on the across-wind fluctuating aerodynamic forces because the ribs suppress large vortex shedding at both sides of the building and simultaneously induce small vortices behind the ribs.

6. Conclusions

The effects of ribs on the local wind pressure coefficients and overall aerodynamic forces of a super high-rise building were surveyed based on wind pressure wind tunnel tests and high-frequency force balance wind tunnel tests on a rigid model. The following conclusions were drawn:

- The ribs block the airflow blow tangentially along the windward facades when wind blows along a body axis of the building, suppressing the decay of positive pressures in the edge regions of the windward facade; therefore, the wind pressure of the whole windward facade increases.
- Ribs can decrease the high suction coefficients in the windward corner recession regions and windward edge regions of the sideward facades when wind blows along a body axis of the building because they suppress vortex shedding at both sides of the building.
- Ribs increase the low fluctuating wind pressure coefficients in the leeward region of the sideward facades, leeward corner recession regions and leeward facades when wind blows along a body axis of the building because they induce small vortices behind them.
- Ribs weaken the most unfavorable suction coefficients by up to 26% in the edge regions of the facades and the corner recession regions. However, there is no obvious influence on the most unfavorable negative wind pressure at the middle part of the facades.
- The ribs have no effect on the most unfavorable positive wind pressure coefficients of high-rise buildings.
- The vertical ribs of high-rise building increase the overall mean aerodynamic forces for along and oblique wind because the ribs increase the low positive mean wind pressure in the edge regions of the windward facade; the ribs on the sideward facades create additional aerodynamic forces for the building. The rates of increase of the mean aerodynamic forces for

along wind are generally between 10%~30%. The maximum mean aerodynamic forces for oblique wind has an increase rates of approximately 10%.

- Ribs increase the along-wind fluctuating aerodynamic forces in most conditions. The maximum value of the increasing rate is 40%. The ribs may increase or decrease the across-wind fluctuating aerodynamic forces. The impact range is approximately 10%.

Acknowledgments

The authors are very grateful for the support provided by the National Natural Science Foundation of China (Grant Nos. 51278367, 50878159 and 91215302).

References

Cook, N.J. and Mayne, J.R. (1980), "A refined working approach to the assessment of wind loads for equivalent static design", *J. Wind Eng. Ind. Aerod*., **6**(1), 125-137.

GB50009, M. (2012), "Load code for the design of building structures", *Ministry of Housing and Urban-Rural Construction of the People's Republic of China, Haidian District, Beijing, China*.

Gu, M., Cao, H. and Quan, Y. (2014), "Experimental study of across-wind aerodynamic damping of super high-rise buildings with aerodynamically modified square cross-sections", *Struct. Des. Tall Spec*., **23**(16), 1225-1245.

Gu, M. and Quan, Y. (2004), "Across-wind loads of typical tall buildings", *J. Wind Eng. Ind. Aerod*., **92**(13), 1147-1165.

Holmes, J.D. (2015), *Wind loading of structures*, CRC Press.

Huang, G., Luo, Y., Gurley, K.R. and Ding, J. (2016), "Revisiting moment-based characterization for wind pressures", *J. Wind Eng. Ind. Aerod.*, **151** 158-168.

Kawai, H. (1998), "Effect of corner modifications on aeroelastic instabilities of tall buildings", *J. Wind Eng. Ind. Aerod*., **74** 719-729.

Kim, Y. and Kanda, J. (2010), "Characteristics of aerodynamic forces and pressures on square plan buildings with height variations", *J. Wind Eng. Ind. Aerod.*, **98**(8), 449-465.

Kim, Y. and Kanda, J. (2010), "Effects of taper and set-back on wind force and wind-induced response of tall buildings", *Wind Struct*.,**13**(6), 499-517.

Kwok, K. (1988), "Effect of building shape on wind-induced response of tall building", *J. Wind Eng. Ind. Aerod*., **28**(1-3), 381-390.

Kwok, K., Wilhelm, P. and Wilkie, B. (1988), "Effect of edge configuration on wind-induced response of tall buildings", *Eng. Struct*.,**10**(2), 135-140.

Naudascher, E., Weske, J. and Fey, B. (1981), "Exploratory study on damping of galloping vibrations", *J. Wind Eng. Ind. Aerod*., **8**(1-2), 211-222.

Quan, Y., Gu, M. and Tamura, Y. (2005), "Experimental evaluation of aerodynamic damping of square super high-rise buildings", *Wind Struct.*, **8**(5), 309-324.

Quan, Y., Gu, M., Tamura, Y. and Chen, B. (2009), "An extreme value estimating method of non-gaussian wind pressure", *Proceedings of the 7th Asia-Pacific Conference on Wind Engineering*, Taipei, Taiwan, November 8-12.

Quan, Y., Kuang, J., Gu, M. and Wang, S. (2015), "Effects of grid curtains on the wind loads of a high-rise building", *Struct. Des. Tall Spec*., **25**(5), 245-262.